Title
Molecular Dynamics Simulations of Perylenediimide DNA Base Surrogates

Journal
The Journal of Physical Chemistry B, 119(35)

ISSN
1520-6106

Authors
Markegard, Cade B
Mazaheripour, Amir
Jocson, Jonah-Micah
et al.

Publication Date
2015-09-03

DOI
10.1021/acs.jpcb.5b03874

Peer reviewed

THE JOURNAL OF PHYSICAL CHEMISTRY B

Article

pubs.acs.org/JPCB

Molecular Dynamics Simulations of Perylenediimide DNA Base Surrogates

Cade B. Markegard,[†] Amir Mazaheripour,[†] Jonah-Micah Jocson,[†] Anthony M. Burke,[†] Mary N. Dickson,[†] Alon A. Gorodetsky,*[,†,‡] and Hung D. Nguyen*[,†]

[†]Department of Chemical Engineering and Materials Science and [‡]Department of Chemistry, University of California, Irvine, Irvine, California 92697, United States

Supporting Information

ABSTRACT: Perylene-3,4,9,10-tetracarboxylic diimides (PTCDIs) are a well-known class of organic materials. Recently, these molecules have been incorporated within DNA as base surrogates, finding ready applications as probes of DNA structure and function. However, the assembly dynamics and kinetics of PTCDI DNA base surrogates have received little attention to date. Herein, we employ constant temperature molecular dynamics simulations to gain an improved understanding of the assembly of PTCDI dimers and trimers. We also use replica-exchange molecular dynamics simulations to elucidate the energetic landscape dictating the formation of stacked PTCDI structures. Our studies provide insight into the equilibrium configurations of multimeric PTCDIs and hold implications for the construction of DNA-inspired systems from perylene-derived organic semiconductor building blocks.

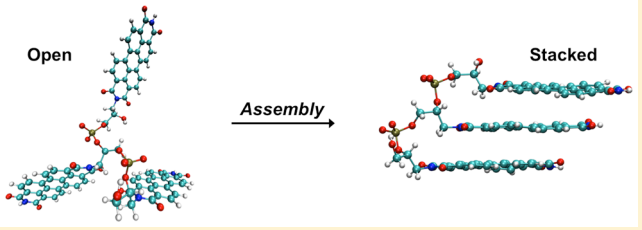

INTRODUCTION

Perylene-3,4,9,10-tetracarboxylic diimide (PTCDI or perylenediimide) derivatives constitute a well-known and extensively studied class of organic materials.[1−8] Due to their tunable coloration and excellent stability, PTCDIs have found ready applications as industrial dyes and pigments.[1,2] Moreover, PTCDIs' favorable electrochemical, photophysical, and self-assembly properties have facilitated not only the fundamental study of charge transport phenomena but also the development of various organic electronic devices, such as transistors and solar cells.[3−8] Consequently, a number of synthetic methodologies have been developed for modulating the properties of PTCDIs.[2,7,8] For example, substitution of these molecules' aromatic core and imide positions provides a degree of control over their electronic properties and self-assembly behavior, respectively.[8] Thus, given the various advantageous features of PTCDIs, it is not surprising that they have attracted much attention from both industry and academia for over 100 years.[1−8]

Due to the widespread interest in the properties and applications of PTCDIs, these molecules have been investigated via computational techniques within certain contexts.[5,9−14] For example, various studies have used density functional theory to establish relationships between the solid state packing and emergent electronic functionality of various substituted PTCDIs.[5,9−13] Moreover, a handful of reports have used molecular dynamics simulations to understand the aggregation and assembly dynamics of PTCDIs both in solution and in the solid state.[5,11−14] These efforts have afforded fundamental insight that is valuable for the design of improved PTCDI-based materials.

Recently, Wagenknecht and co-workers have developed a new class of PTCDI derivatives for use as artificial DNA base surrogates.[15−20] Within the context of standard oligonucleotide synthesis, such derivatives are advantageous because they can be incorporated in arbitrary positions within the DNA base pair stack in high yield.[15−26] To date, these molecules have been used for a number of applications, including the assembly of higher-order DNA ensembles,[20−22] the photophysical investigation of DNA structure/function,[16,17,19] the study of charge transfer in DNA hairpins,[23−25] and the electrochemical interrogation of DNA monolayers.[26] However, the assembly dynamics and kinetics of PTCDI DNA base surrogates have not been extensively explored via computational techniques.[21,22]

Herein, we present a molecular dynamics study of multimeric PTCDI DNA base surrogates. We first design, synthesize, and characterize model oligonucleotides featuring one, two, and three covalently attached PTCDI moieties. We then parametrize the oligonucleotides' PTCDI subunits and formulate an atomistic model of these constructs. We subsequently employ constant-temperature molecular dynamics simulations to develop an improved understanding of the assembly kinetics of PTCDI dimers and trimers. We in turn perform replica exchange molecular dynamics simulations to obtain the energetic landscape associated with ensembles of our stacked PTCDI structures at equilibrium. Altogether, our findings may hold implications for the design of DNA-inspired systems and

Received: April 23, 2015
Revised: July 22, 2015

DOI: 10.1021/acs.jpcb.5b03874
J. Phys. Chem. B XXXX, XXX, XXX−XXX

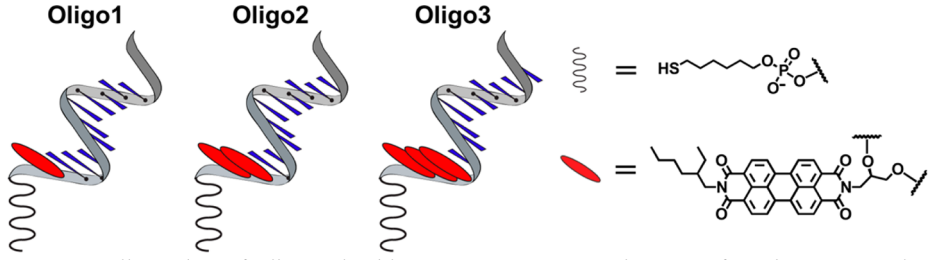

Figure 1. Illustration of oligonucleotides Oligo1, Oligo2, and Oligo3 containing 1, 2, and 3 PTCDI base surrogates (red ovals), respectively. The DNA sequences of these macromolecules were 5′-$(A)_{10}(P)_n$-S-3′, where the A, P, and S indicate the locations of the adenines, PTCDIs, and thiols, respectively, and n corresponds to the number of PTCDIs.

materials from not only PTCDIs but also other organic semiconductor building blocks

EXPERIMENTAL SECTION

Preparation of the DNA Phosphoramidites. The phosphoramidites required for DNA synthesis were purchased from Glen Research, Inc., or Azco Biotech, Inc., and used as received. The perylenediimide phosphoramidites were synthesized and characterized according to established literature protocols.[26] The identity and purity of the perylenediimide phosphoramidites, as well as all intermediates required for their synthesis, were confirmed with ^{1}H NMR, ^{13}C NMR, ^{31}P NMR, and mass spectrometry.[26]

Synthesis, Purification, and Characterization of the Oligonucleotides. The PTDCI-modified oligonucleotides (Figure 1) were prepared according to standard commercial protocols recommended by Glen Research, Inc., for an Applied Biosystems (ABI) 394 DNA synthesizer. Extended coupling times were used for the incorporation of perylenediimide phosphoramidites, as previously described.[26] After synthesis, the oligonucleotides were cleaved from the solid support by treatment with aqueous ammonium hydroxide and purified with high performance liquid chromatography (HPLC) on an Agilent 1260 Infinity system. The oligonucleotides were eluted with a gradient evolved from 95% solvent A and 5% solvent B to 0% solvent A and 100% solvent B over 30 min at a flow rate of 1 mL/min (solvent A, 50 mM ammonium acetate, pH = 6 buffer; solvent B, acetonitrile) on Agilent reverse phase C4 or C8 columns (see Supporting Figure 1 for typical chromatograms). The UV−visible (UV−vis) absorption spectra of the oligonucleotides were obtained with an Agilent 1260 Infinity Series diode array detector during chromatographic purification. The MALDI-TOF mass spectra of the oligonucleotides were recorded on an Applied Biosystems Sciex MALDI-TOF/TOF 5800 series mass spectrometer in reflectron negative mode, using a 349 nm Nd:YAG laser as the illumination source and 3-hydroxypicolinic acid as the matrix (see Supporting Figure 2 for typical spectra).

Parameterization of the Perylenediimide Base Surrogates. For the simulations, three separate residues containing terminal phosphate moieties were designed according to established literature protocols (Supporting Figure 3).[27] The chemical structures of the residues were exported as mol2 files from ChemDraw 13.0, and these structures were initially optimized using molecular mechanics in Gaussian 09.[28] The geometry optimization was completed in Gaussian 09 with the Hartree−Fock method and the 6-31G(d) basis set, via the methodology previously reported for the Generalized AMBER Force Field (GAFF).[28,29]

After convergence of the structures, the atomic point charges for the three residues were determined via the two-step Restricted Electrostatic Potential (RESP) method (Supporting Figure 4 and Supporting Tables 1−3). The residues' electrostatic potentials were first calculated in Gaussian 09, and the Merz−Kollman scheme was used to correctly output the log file for AMBER's *antechamber*.[29] Next, atom typing was completed by *antechamber*, and the resulting charges were appended into mol2 files. The mol2 files were in turn imported into *xleap* by using the GAFF force field parameters. To form multimeric PTCDI constructs for the subsequent molecular dynamics simulations, the residues were appended in *xleap*,[29−31] with the redundant terminal phosphate moieties removed.[27] Note that charge constraints were enforced according to established literature precedent for parametrization of DNA residues in AMBER.[27]

Molecular Dynamics Simulations of the Perylenediimide Base Surrogate Stacking Kinetics. Molecular dynamics simulations of PTCDI stacking kinetics (20 total) were performed with GAFF in NAMD 2.9.[32,33] The simulations employed the Generalized Born Implicit Solvent model (GBIS) and a monovalent salt concentration of 0.115 M.[32,33] For each simulation, the starting configuration was obtained by turning off the attractive van der Waals interactions in the force field and setting the temperature to 500 K, thereby ensuring that all PTCDI moieties were completely separated from one another in an unstacked random open configuration. To initiate the simulation, the attractive van der Waals interactions were turned on and the initial temperature was set to 300 K. All of the simulations were performed at a constant temperature of 300 K for 20 ns, ensuring that steady state was reached. The simulations were analyzed by monitoring the relative center of mass (COM) distances and offset angles for every pair of PTCDIs. The COM distances were calculated from the atomic coordinates and atomic mass of the individual PTCDIs. Here, the offset angles were obtained by constructing a vector from the nitrogen closest to the backbone to the nitrogen farthest from the backbone for the individual PTCDIs (Supporting Figure 5). The dot product of these vectors for every pair of PTCDIs defined the offset angles used for the analysis. The COM distances and offset angles indicated the relative separation and alignment of the PTCDIs, respectively. As an example, if the COM distance of two PTCDIs is ∼3.4 Å and their offset angle is 0°, the two molecules are stacked and perfectly aligned on top of one another (Supporting Figure 6). The simulations also yielded the van der Waals and electrostatic interactions for each pair of PTCDIs. These interactions were monitored as a function of time to gain insight into the factors driving the self-assembly of PTCDI ensembles.

DOI: 10.1021/acs.jpcb.5b03874
J. Phys. Chem. B XXXX, XXX, XXX−XXX

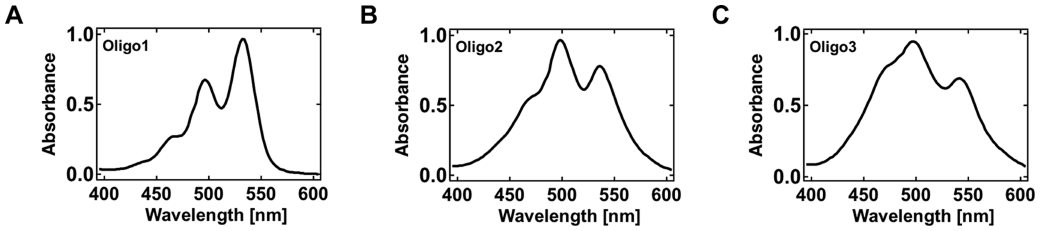

Figure 2. Normalized UV−vis absorption spectra obtained for Oligo1, Oligo2, and Oligo3 containing 1, 2, and 3 PTCDIs, respectively. Note the change in the relative intensities of the absorption peaks for Oligo2 and Oligo3 compared to Oligo1.

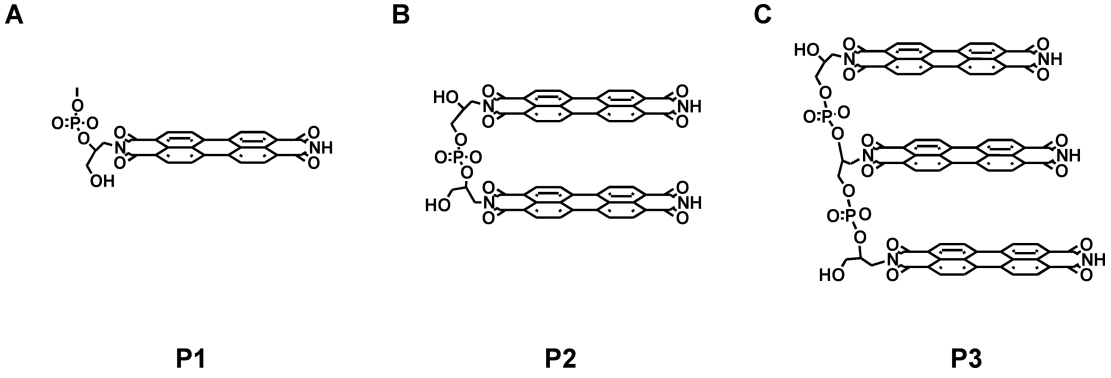

Figure 3. Chemical structures of the PTCDI subunits used for the molecular dynamics simulations. The subunits are labeled as P1, P2, and P3, and they correspond to Oligo1, Oligo2, and Oligo3, respectively.

Replica-Exchange Molecular Dynamics Simulations of Perylenediimide Base Surrogate Assembly. Replica exchange molecular dynamics (REMD) simulations were performed to explore the energetic landscape of the oligonucleotides' stacked PTCDI subunits.[34] The simulations were run for 16 replicates distributed over a temperature range of 290 to 700 K. The simulation time was 320 ns per replica, corresponding to 80,000 total exchanges, with an exchange attempt every 4 ps. The simulations generated the equilibrium atomic structures for an ensemble of the PTCDI subunits. These structures were analyzed via the MBAR method, enabling calculation of the potential of mean force (PMF) for the stacked PTCDIs as a function of their COM distances and offset angles.[35] This analysis yielded the free energy landscapes of our constructs at 300 K.

RESULTS AND DISCUSSION

We began our experiments by designing the series of model PTCDI-containing macromolecules shown in Figure 1 (Oligo1, Oligo2, and Oligo3). These macromolecules incorporated 1 to 3 PTCDI moieties, an alkanethiol functionality at their 3′ end, and a polyadenine tract at their 5′ end (the terminal modifications were included to mitigate intermolecular aggregation). Because bulky PTCDIs are typically placed either at terminal positions or opposite abasic sites within duplex DNA,[15−26] we specifically focused our efforts on the preparation and analysis of single stranded DNA. Indeed, upon binding the 3′ polyadenine tract of our constructs, the complementary strands would be expected to exhibit a relatively small effect on the rapid assembly dynamics and kinetics of the terminal PTCDI DNA base surrogates. Overall, Oligo1, Oligo2, and Oligo3 represented reasonable general analogues for the diverse class of perylene-modified oligonucleotides previously investigated with photophysical techniques in solution[16,17,19] and electrochemical techniques at solid substrates.[26]

We characterized Oligo1, Oligo2, and Oligo3 with UV−vis spectroscopy (Figure 2), observing a clear evolution in the molecules' spectra as the number of PTCDI moieties increased. For Oligo1, the spectrum of DNA1 was indicative of a single, isolated PTCDI, with three characteristic absorption peaks of successively increasing intensity at 466, 496, and 534 nm (Figure 2). However, the situation was markedly different for Oligo2 and Oligo3. Although the absorption peaks maintained similar positions, the spectra were broadened, with the absorption peaks at 498 nm for Oligo2 and 497 nm for Oligo3 now exhibiting the largest relative intensities. This type of evolution in our constructs' UV−vis spectra was indicative of strong pi−pi stacking interactions between the adjacent PTCDIs.[2−8,36]

With our model constructs in hand, we proceeded to perform constant temperature molecular dynamics simulations for the PTCDI subunits of Oligo2 and Oligo3 (Figure 3). For simplicity, we only considered the structures shown in Figure 3 (denoted as P1, P2, and P3), removing the alkyl tails on the PTCDIs, the 3′ alkanethiol functionalities, the 5′ polyadenine tracts, and the terminal phosphate groups (when appropriate). We leveraged established literature protocols previously developed for oligonucleotides and DNA to parametrize the PTCDI moieties with the Generalized AMBER Force Field, facilitating the computational analysis.[29−31] Here, through our simulations, we anticipated gaining insight into both the kinetics of self-assembly and the ultimate geometries for P2 and P3.

We initially investigated the kinetics of self-assembly for the two PTCDI moieties of P2, as illustrated for a typical simulation in Figure 4. At t = 0.051 ns, the two PTCDIs maintained a random open configuration (Figure 4A), with a COM distance of 18.34 Å (Figure 4E) and an offset angle of 125.7° (Figure 4F). After 1.718 ns, the top PTCDI had started

DOI: 10.1021/acs.jpcb.5b03874
J. Phys. Chem. B XXXX, XXX, XXX−XXX

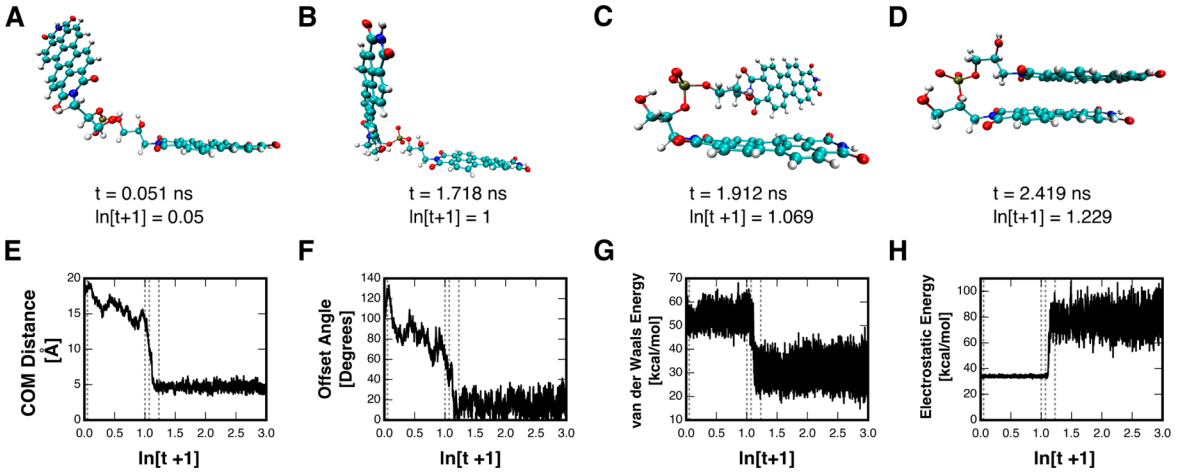

Figure 4. Snapshots of P2 during a molecular dynamics simulation at times of (A) t = 0.051 ns, (B) t = 1.718 ns, (C) t = 1.912 ns, and (D) t = 2.419 ns. The sequence demonstrates the transition of P2 from an open random configuration to a stacked configuration. (E) The evolution of the centers of mass (COM) distance between the two PTCDIs of P2 as a function of time. (F) The evolution of the offset angle between the two PTCDIs of P2 as a function of time. (G) The evolution of the van der Waals energy of P2 as a function of time. (H) The evolution of the electrostatic energy of the PTCDIs' carbonyl oxygens distal to the alkane phosphate backbone as a function of time. The four vertical dashed lines in E, F, G, and H correspond to the times used for the snapshots in A, B, C, and D. The simulations were performed at a constant temperature of 300 K.

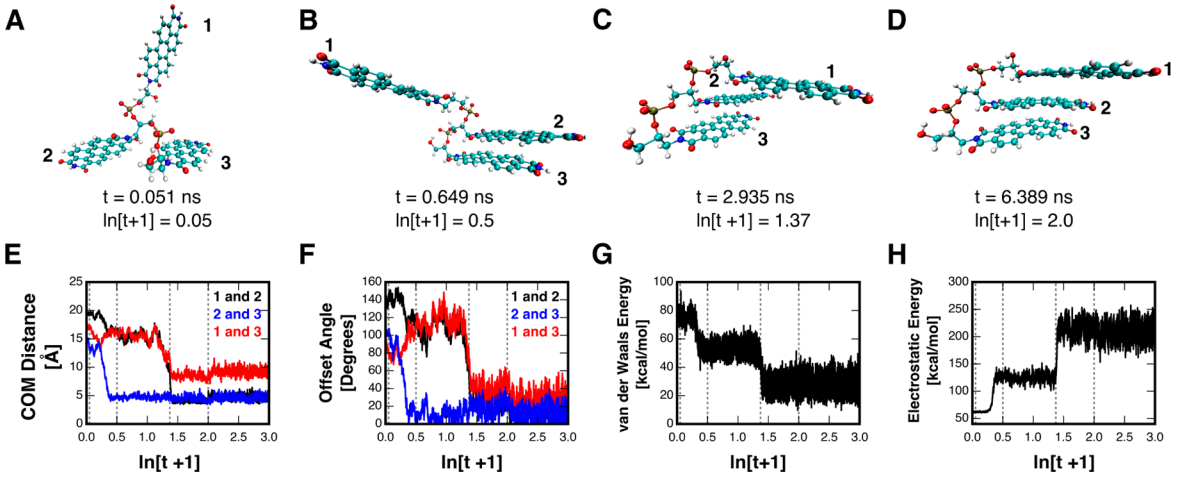

Figure 5. Snapshots of P3 during a molecular dynamics simulation at times of (A) t = 0.051 ns, (B) t = 0.649 ns, (C) t = 2.935 ns, and (D) t = 6.389 ns. The constituent PTCDIs of P3 are labeled as **1**, **2**, and **3**. The sequence demonstrates the transition of P3 from an open random configuration to a stacked configuration. (E) The evolution of the centers of mass (COM) distance between PTCDIs **1** and **2** (black curve), PTCDIs **2** and **3** (blue curve), and PTCDIs **1** and **3** (red curve) as a function of time. (F) The evolution of the offset angle between PTCDIs **1** and **2** (black curve), PTCDIs **2** and **3** (blue curve), and PTCDIs **1** and **3** (red curve) as a function of time. (G) The evolution of the van der Waals energy of P3 as a function of time. (H) The evolution of the electrostatic energy of the PTCDIs' carbonyl oxygens distal to the alkane phosphate backbone as a function of time. The four vertical dashed lines in E, F, G, and H correspond to the times used for the snapshots in A, B, C, and D. The simulations were performed at a constant temperature of 300 K.

to flip (Figure 4B), leading to a slight decrease in the COM distance to 14.34 Å (Figure 4E) and a reduction in the offset angle to 68.28° (Figure 4F). After 1.912 ns, the top PTCDI had begun to orient itself toward the bottom PTCDI (Figure 4C), leading to a further decrease in the COM distance (Figure 4E) and an additional reduction in the offset angle (Figure 4F). Finally, after 2.419 ns, the two PTCDIs had collapsed to a stacked state (Figure 4D), with an average COM distance of 4.6 Å (Figure 4E) and an average offset angle of 15.51° (Figure 4F). Here, although the two PTCDIs remain stacked for the remainder of the ∼20 ns simulation, their COM distances and offset angles varied by ∼0.44 Å and ∼7.83°, respectively. Such geometric variability likely resulted from thermal fluctuations, hinting at some dynamic character for the final configuration. Nonetheless, the final stacked dimer was highly reproducible, with nearly identical results obtained for ten independent repetitions.

To gain additional insight into the self-assembly of P2's PTCDI moieties, we analyzed the energetics driving this process. When the two PTCDIs collapsed to a stacked configuration between ∼1.9 ns and ∼2.4 ns (Figure 4E,F), there was a sharp decrease in the van der Waals energy of the system, due to pi−pi interactions between the molecules' aromatic cores (Figure 4G), and a sharp increase in the electrostatic energy, due to repulsion between the PTCDIs' carbonyl groups located distal to the alkane phosphate backbone (Figure 4H). The competition between these two sets of interactions appeared to dictate the final arrangement of the system, where there was substantial overlap between the

DOI: 10.1021/acs.jpcb.5b03874
J. Phys. Chem. B XXXX, XXX, XXX−XXX

perylene cores but a misalignment of the carbonyl groups (Figure 4D).

We next investigated the kinetics of self-assembly for the three PTCDI moieties of P3. In our experiments, we observed that the formation of P3's final arrangement required a two-step mechanism. First, two of the PTCDIs formed a dimer analogous to the one found for the final configuration of P2. Second, the remaining third PTCDI stacked with this dimer to form a trimer. Although our simulations revealed multiple possibilities for the PTCDIs' stacking order (Figure 5 and Supporting Figures 7 and 8), this general mechanism was highly reproducible, with similar results obtained for ten independent simulations.

As an example, Figure 5 shows a typical P3 stacking kinetics simulation, which demonstrates the aforementioned multistep mechanism and the most likely assembly pathway. At t = 0.051 ns, the three constituent PTCDIs (denoted as **1**, **2**, and **3**) were unstacked with a random open configuration (Figure 5A). Initially, as illustrated by the snapshot at t = 0.649 ns (Figure 5B), **2** and **3** formed a dimer during the first step of the stacking mechanism. There was a corresponding sharp drop from 13.34 to 5.02 Å in the COM distance (Figure 5E) and from 100.61° to 1.30° in the offset angle (Figure 5F) between **2** and **3**. In turn, as illustrated by the snapshot at t = 2.935 ns (Figure 5C), **1** stacked on top of the dimer to form a trimer during the second step of the stacking mechanism. For this step, there was a sharp drop from 9.09 to 5.61 Å in the COM distance (Figure 5E) and from 63.26° to 13.76° in the offset angle (Figure 5F) between **1** and **2**. There also was an accompanying drop from 10.92 to 9.29 Å in the COM distance (Figure 5E) and from 73.07° to 30.45° in the offset angle (Figure 5F) between **1** and **3**. Although the three PTCDIs remained in a stacked arrangement for the remainder of the ∼20 ns simulation, as illustrated by the snapshot at t = 6.389 ns (Figure 5D), we again observed variability in their relative COM distances and offset angles (Figure 5E,F), indicating some dynamic character for the final configuration.

To further understand the self-assembly of P3's PTCDI moieties, we analyzed the energetics dictating the overall process. In the first step of the mechanism, the formation of the dimer was driven by a sharp decrease in the van der Waals energy of the system, due to pi−pi interactions between the molecules' aromatic cores (Figure 5G), and a sharp increase in the electrostatic energy, due to repulsion between the PTCDIs' carbonyl groups located distal to the alkane phosphate backbone (Figure 5H), as also observed for P2 above (Figure 4G,H). In the second step of the mechanism, a similar interplay of favorable and unfavorable interactions appeared to drive formation of the trimer, as indicated by similar changes in the van der Waals and electrostatic energies (Figure 5G,H). These competing interactions ensured that the three constituent PTCDIs of P3 adopted a twisted arrangement in the final equilibrium configuration, where they were stacked but offset with respect to one another (Figure 5D).

We proceeded to perform REMD simulations for P2 and P3. Relative to constant temperature simulations, REMD simulations are advantageous because they minimize the possibility of kinetic traps.[34] Moreover, replica exchange simulations enable direct calculation of the potential of mean force (PMF), facilitating comparisons between the relative free energies of different equilibrium structures.[35] Here, through such simulations, we anticipated gaining insight into the distinct configurations possible for P2 and P3 over a broad temperature window.

We performed REMD simulations for P2, obtaining equilibrium structures such as the one illustrated in Figure 6A,B. These configurations spanned a range of COM distance

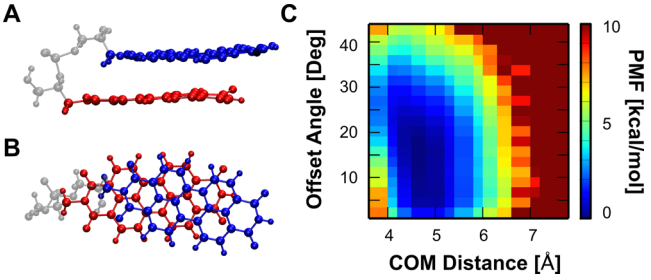

Figure 6. Snapshots of the lowest energy equilibrium structure observed for P2 from (A) a side view and (B) a top view. The backbone is colored gray, and the two PTCDIs are colored red and blue. (C) The potential of mean force (PMF) in kcal/mol as a function of both the centers of mass (COM) distance and the offset angle between the two PTCDIs of P2, as obtained from a replica exchange simulation at 300 K.

and average offset angle combinations, corresponding to various PMF values (Figure 6C). As a general rule, the low free energy structures found for P2 featured COM distances between 4.2 and 5.2 Å and offset angles between 3° and 22°. For example, the lowest energy equilibrium structure shown in Figure 6A,B featured a COM distance of 4.53 Å and an offset angle of 14.61°, in excellent agreement with the kinetic simulations above. Notably, configurations with COM distances of >∼7 Å possessed large free energies, underscoring the PTCDIs' known propensity for stacking.[2−8] However, configurations with COM distances of ∼3.4 Å and offset angles close to 0° still possessed large free energies, indicating that perfect overlap of the two PTCDIs was not favored. Overall, these simulations provided additional insight into the preferred equilibrium arrangement of the PTCDI moieties of P2.

We subsequently performed REMD simulations for P3, obtaining equilibrium structures such as the one illustrated in Figure 7A,B. These simulations again yielded an ensemble of possible P3 configurations, which we analyzed by comparing the relative orientations of the three constituent PTCDIs (denoted as **1**, **2**, and **3**). The possible COM distance and offset angle combinations obtained for **1** and **2**, along with their corresponding PMF values, are illustrated in Figure 7C, and the possible COM distance and offset angle combinations obtained for **2** and **3**, along with their corresponding PMF values, are illustrated in Figure 7D. As observed for P2, the equilibrium structures with the lowest free energies featured COM distances between 4.2 and 5.2 Å and offset angles between 3° and 22°. For example, the lowest energy equilibrium structure shown in Figure 7C,D featured a COM distance of 4.86 Å and an offset angle of 6.01° for **1** and **2**, as well as a COM distance of 5.24 Å and an offset angle of 4.5° for **2** and **3**. Although the three PTCDIs comprising this structure adopted a stacked arrangement, they did not overlap perfectly and were slightly offset with respect to one another. These findings were again in agreement with the kinetics simulations and afforded an improved understanding of the energetic landscape dictating the self-assembly of P3.

DOI: 10.1021/acs.jpcb.5b03874
J. Phys. Chem. B XXXX, XXX, XXX−XXX

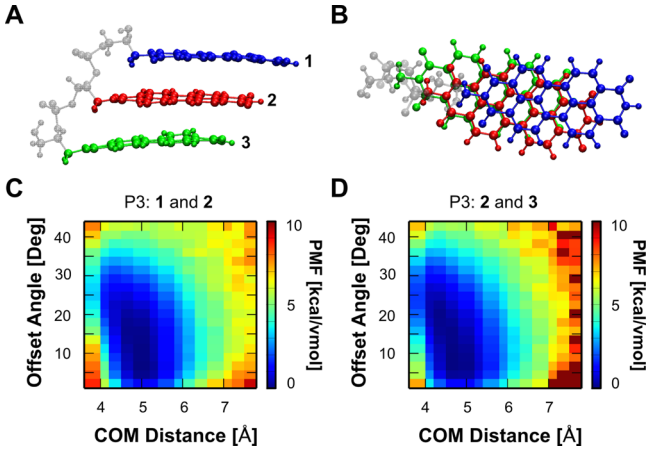

Figure 7. Snapshots of the lowest energy equilibrium structure observed for P3 from (A) a side view and (B) a top view. The backbone is colored gray, and PTCDIs **1**, **2**, and **3** are colored blue, red, and green, respectively. (C) The potential of mean force (PMF) in kcal/mol as a function of both the centers of mass (COM) distance and the offset angle between PTCDIs **1** and **2** of P3, as obtained from a replica exchange simulation at 300 K. (D) The potential of mean force (PMF) in kcal/mol as a function of both the center of mass (COM) distance and the offset angle between PTCDIs **2** and **3** of P3, as obtained from a replica exchange simulation at 300 K.

Finally, our REMD simulations indicated that the PTCDI moieties comprising the P2 and P3 equilibrium structures were nonplanar on short time scales (Figure 6A,B and Figure 7A,B). To gain insight into the origin of this effect, we compared the distortion from planarity found for the stacked, interacting PTCDIs of P2 and P3 with the distortion from planarity found for the independent PTCDI of P1. For this comparison, we defined a bend angle between two vectors from the center to the edge of the PTCDIs (Supporting Figure 9). The PTCDI of P1 featured a range of bend angles between 153.27° and 179.92°, with an average value of 174.66 ± 3.67° (Supporting Figure 9). Interestingly, we found that the PTCDIs of P2 and P3 all featured nearly identical bending angle distributions (Supporting Figures 10 and 11). Given that the average distortions were small and not dependent on stacking interactions, we postulated that the observed deviations from planarity were likely due to thermal fluctuations. These findings further underscored the rich dynamics of stacked PTCDIs, which warrant additional exploration.

CONCLUSION

In summary, we have used constant temperature and replica exchange molecular dynamics simulations to investigate the self-assembly of covalently linked perylene-3,4,9,10-tetracarboxylic diimide DNA base surrogates. Together, our computational analyses yielded insight not readily apparent from experimental methodologies and were significant for several reasons. First, to the best of our knowledge, the stacking kinetics of PTCDI DNA base surrogates have received little attention from a computational perspective, especially with regard to investigating the process in its entirety. Second, our simulations have allowed for observation of the assembly kinetics in atomistic detail, revealing that the underlying mechanism is quite complex and may encompass multiple distinct pathways. Third, our studies have unveiled the energetics of multimeric PTCDI ensembles, indicating that a complex interplay of attractive van der Waals and repulsive electrostatic interactions dictates their assembly and final structures. Fourth, the simulations demonstrate that the observed equilibrium structures are not fully static and possess some dynamic character, as evidenced by fluctuations in the relative positions and planarity of the stacked PTCDIs. Fifth, the presented computational framework is quite general and can be readily extended to the study of more complex sequence- and length-variable systems consisting of covalently linked pi-conjugated organic semiconductor building blocks. Overall, our studies constitute a foundation for the rational design and construction of precisely defined one-dimensional nanowires that draw inspiration from the structure of DNA.

ASSOCIATED CONTENT

Supporting Information

The Supporting Information is available free of charge on the ACS Publications website at DOI: 10.1021/acs.jpcb.5b03874.

Experimental and simulation data (PDF)

AUTHOR INFORMATION

Corresponding Authors

*E-mail: alon.gorodetsky@uci.edu.

*E-mail: hdn@uci.edu.

Notes

The authors declare no competing financial interest.

ACKNOWLEDGMENTS

A.A.G. was supported by the Air Force Office of Scientific Research (FA9550-13-1-0096) and the National Science Foundation (CMMI-1246762). The computational studies used the Extreme Science and Engineering Discovery Environment (XSEDE), which is supported by the National Science Foundation (OCI-1053575). We are also grateful for the computational resources provided by the GreenPlanet High Performance Computing cluster available at the University of California, Irvine.

REFERENCES

(1) Herbst, W.; Hunger, K. *Industrial Organic Pigments: Production, Properties, Applications*, 2nd ed.; Wiley: Weinheim, 1997.

(2) Würthner, F. Perylene Bisimide Dyes as Versatile Building Blocks for Functional Supramolecular Architectures. *Chem. Commun.* **2004**, 1564−1579.

(3) Li, C.; Wonneberger, H. Perylene Imides for Organic Photovoltaics: Yesterday, Today, and Tomorrow. *Adv. Mater.* **2012**, *24*, 613−636.

(4) Görl, D.; Zhang, X.; Würthner, F. Molecular Assemblies of Perylene Bisimide Dyes in Water. *Angew. Chem., Int. Ed.* **2012**, *51*, 6328−6348.

(5) Geng, Y.; Li, H.-B.; Wu, S.-X.; Su, Z.-M. The Interplay of Intermolecular Interactions, Packing Motifs and Electron Transport Properties in Perylene Diimide Related Materials: a Theoretical Perspective. *J. Mater. Chem.* **2012**, *22*, 20840−20851.

(6) Kozma, E.; Catellani, M. Perylene Diimides Based Materials for Organic Solar Cells. *Dyes Pigm.* **2013**, *98*, 160−179.

(7) Jung, B. J.; Tremblay, N. J.; Yeh, M.-L.; Katz, H. E. Molecular Design and Synthetic Approaches to Electron-Transporting Organic Transistor Semiconductors. *Chem. Mater.* **2011**, *23*, 568−582.

(8) Huang, C.; Barlow, S.; Marder, S. R. Perylene-3,4,9,10-tetracarboxylic Acid Diimides: Synthesis, Physical Properties, and Use in Organic Electronics. *J. Org. Chem.* **2011**, *76*, 2386−2407.

(9) Vura-Weis, J.; Ratner, M. A.; Wasielewski, M. R. Geometry and Electronic Coupling in Perylenediimide Stacks: Mapping Structure-

DOI: 10.1021/acs.jpcb.5b03874
J. Phys. Chem. B XXXX, XXX, XXX−XXX

Charge Transport Relationships. *J. Am. Chem. Soc.* **2010**, *132*, 1738−1739.
(10) Delgado, M. C. R.; Kim, E.-G.; da Silva Filho, D. A.; Bredas, J.-L. Tuning the Charge-Transport Parameters of Perylene Diimide Single Crystals via End and/or Core Functionalization:·A Density Functional Theory Investigation. *J. Am. Chem. Soc.* **2010**, *132*, 3375−3387.
(11) Marcon, V.; Breiby, D. W.; Pisula, W.; Dahl, J.; Kirkpatrick, J.; Patwardhan, S.; Grozema, F.; Andrienko, D. Understanding Structure-Mobility Relations for Perylene Tetracarboxydiimide Derivatives. *J. Am. Chem. Soc.* **2009**, *131*, 11426−11432.
(12) May, F.; Marcon, V.; Hansen, M. R.; Grozema, F.; Andrienko, D. Relationship between Supramolecular Assembly and Charge-Carrier Mobility in Perylenediimide Derivatives: the Impact of Side Chains. *J. Mater. Chem.* **2011**, *21*, 9538−9545.
(13) Idé, J.; Méreau, R.; Ducasse, L.; Castet, F.; Olivier, Y.; Martinelli, N.; Cornil, J.; Beljonne, D. Supramolecular Organization and Charge Transport Properties of Self-Assembled π-π Stacks of Perylene Diimide Dyes. *J. Phys. Chem. B* **2011**, *115*, 5593−5603.
(14) Teklebrhan, R. B.; Ge, L.; Bhattacharjee, S.; Xu, Z.; Sjöblom, J. Probing Structure−Nanoaggregation Relations of Polyaromatic Surfactants: A Molecular Dynamics Simulation and Dynamic Light Scattering Study. *J. Phys. Chem. B* **2012**, *116*, 5907−5918.
(15) Wagner, C.; Wagenknecht, H.-A. Perylene-3,4:9,10-tetracarboxylic Acid Bisimide Dye as an Artificial DNA Base Surrogate. *Org. Lett.* **2006**, *8*, 4191−4194.
(16) Baumstark, D.; Wagenknecht, H.-A. Fluorescent Hydrophobic Zippers Inside Duplex DNA: Interstrand Stacking of Perylene-3,4:9,10-tetracarboxylic Acid Bisimides as Artificial DNA Base Dyes. *Chem. - Eur. J.* **2008**, *14*, 6640−6645.
(17) Baumstark, D.; Wagenknecht, H.-A. Perylene Bisimide Dimers as Fluorescent "Glue" for DNA and for Base-Mismatch Detection. *Angew. Chem., Int. Ed.* **2008**, *47*, 2612−2614.
(18) Menacher, F.; Wagenknecht, H.-A. Synthesis of DNA with Green Perylene Bisimides as DNA Base Substitutions. *Eur. J. Org. Chem.* **2011**, *24*, 4564−4570.
(19) Menacher, F.; Wagenknecht, H.-A. Ratiometric Molecular Beacons Based on the Perylene Bisimide as a Dimeric Internal DNA Base Substitution. *Photochem. Photobiol. Sci.* **2011**, *10*, 1275−1278.
(20) Menacher, F.; Stepanenko, V.; Würthner, F.; Wagenknecht, H.-A. Assembly of DNA Triangles Mediated by Perylene Bisimide Caps. *Chem. - Eur. J.* **2011**, *17*, 6683−6688.
(21) Zheng, Y.; Long, H.; Schatz, G. C.; Lewis, F. D. Duplex and Hairpin Dimer Structures for Perylene Diimide−Oligonucleotide Conjugates. *Chem. Commun.* **2005**, *38*, 4795−4797.
(22) Hariharan, M.; Zheng, Y.; Long, H.; Zeidan, T. A.; Schatz, G. C.; Vura-Weis, J.; Wasielewski, M. R.; Zuo, X.; Tiede, D. M.; Lewis, F. D. Hydrophobic Dimerization and Thermal Dissociation of Perylenediimide-Linked DNA Hairpins. *J. Am. Chem. Soc.* **2009**, *131*, 5920−5929.
(23) Zeidan, T. A.; Carmieli, R.; Kelley, R. F.; Wilson, T. M.; Lewis, F. D.; Wasielewski, M. R. Charge-Transfer and Spin Dynamics in DNA Hairpin Conjugates with Perylenediimide as a Base-Pair Surrogate. *J. Am. Chem. Soc.* **2008**, *130*, 13945−13955.
(24) Carmieli, R.; Zeidan, T. A.; Kelley, R. F.; Mi, Q.; Lewis, F. D.; Wasielewski, M. R. Excited State, Charge Transfer, and Spin Dynamics in DNA Hairpin Conjugates with Perylenediimide Hairpin Linkers. *J. Phys. Chem. A* **2009**, *113*, 4691−4700.
(25) Wilson, T. M.; Zeidan, T. A.; Hariharan, M.; Lewis, F. D.; Wasielewski, M. R. Electron Hopping Among Cofacially Stacked Perylenediimides Assembled by Using DNA Hairpins. *Angew. Chem., Int. Ed.* **2010**, *49*, 2385−2388.
(26) Wohlgamuth, C. H.; McWilliams, M.; Mazaheripour, A.; Burke, A.; Lin, K.-Y.; Doan, L.; Slinker, J. P.; Gorodetsky, A. A. Electrochemistry of DNA Monolayers Modified with a Perylenediimide Base Surrogate. *J. Phys. Chem. C* **2014**, *118*, 29084−29090.
(27) Cieplak, P.; Cornell, W. D.; Bayly, C.; Kollman, P. A. Application of the Multimolecule and Multiconformational RESP Methodology to Biopolymers: Charge Derivation for DNA, RNA, and Proteins. *J. Comput. Chem.* **1995**, *16*, 1357−1377.
(28) Frisch, M. J.; Trucks, G. W.; Schlegel, H. B.; Scuseria, G. E.; Robb, M. A.; Cheeseman, J. R.; Scalmani, G.; Barone, V.; Mennucci, B.; Petersson, G. A.; et al. *Gaussian 09*, Revision A.1; Gaussian, Inc.: Wallingford, CT, 2009.
(29) Wang, J.; Wolf, R. M.; Caldwell, J. W.; Kollman, P. A.; Case, D. A. Development and Testing of a General Amber Force Field. *J. Comput. Chem.* **2004**, *25*, 1157−1174.
(30) Jakalian, A.; Bush, B. L.; Jack, D. B.; Bayly, C. I. Fast, Efficient Generation of High-Quality Atomic Charges. AM1-BCC Model: I. Method. *J. Comput. Chem.* **2000**, *21*, 132−146.
(31) Jakalian, A.; Jack, D. B.; Bayly, C. I. Fast, Efficient Generation of High-Quality Atomic Charges. AM1-BCC Model: II. Parameterization and validation. *J. Comput. Chem.* **2002**, *23*, 1623−1641.
(32) Darden, T. A.; Cheatham, T. E., III; Simmerling, C. L.; Wang, J.; Duke, R. E.; Luo, R.; Walker, R. C.; Zhang, W.; Merz, K. M.; Roberts, B. et al. *Amber 12*; University of California: San Francisco, CA, 2012.
(33) Phillips, J. C.; Braun, R.; Wang, W.; Gumbart, J.; Tajkhorshid, E.; Villa, E.; Chipot, C.; Skeel, R. D.; Kalé, L.; Schulten, K. Scalable Molecular Dynamics with NAMD. *J. Comput. Chem.* **2005**, *26*, 1781−1802.
(34) Sugita, Y.; Okamoto, Y. Replica-Exchange Molecular Dynamics Method for Protein Folding. *Chem. Phys. Lett.* **1999**, *314*, 141−151.
(35) Shirts, M. R.; Chodera, J. D. Statistically Optimal Analysis of Samples from Multiple Equilibrium States. *J. Chem. Phys.* **2008**, *129*, 124105−124118.
(36) Clark, A. E.; Qin, C.; Li, A. D. Q. Beyond Exciton Theory: A Time-Dependent DFT and Franck-Condon Study of Perylene Diimide and Its Chromophoric Dimer. *J. Am. Chem. Soc.* **2007**, *129*, 7586−7595.

DOI: 10.1021/acs.jpcb.5b03874
J. Phys. Chem. B XXXX, XXX, XXX−XXX